



# Temporal Scattering, Depolarization, and Persistent Radio Emission from Magnetized Inhomogeneous Environments near Repeating Fast Radio Burst Sources

Yuan-Pei Yang<sup>1</sup> , Wenbin Lu<sup>2</sup> , Yi Feng<sup>3</sup> , Bing Zhang<sup>4,5</sup> , and Di Li<sup>6,7</sup> <sup>1</sup> South-Western Institute for Astronomy Research, Yunnan University, Kunming, Yunnan 650500, People's Republic of China; [ypyang@ynu.edu.cn](mailto:ypyang@ynu.edu.cn)<sup>2</sup> Department of Astrophysical Sciences, Princeton University, Princeton, NJ 08544, USA; [wenbinlu@astro.princeton.edu](mailto:wenbinlu@astro.princeton.edu)<sup>3</sup> Zhejiang Lab, Hangzhou, Zhejiang 311121, People's Republic of China<sup>4</sup> Nevada Center for Astrophysics, University of Nevada, Las Vegas, NV 89154, USA<sup>5</sup> Department of Physics and Astronomy, University of Nevada, Las Vegas, NV 89154, USA<sup>6</sup> National Astronomical Observatories, Chinese Academy of Sciences, Beijing 100101, People's Republic of China<sup>7</sup> University of Chinese Academy of Sciences, Beijing 100049, People's Republic of China

Received 2022 February 7; revised 2022 March 9; accepted 2022 March 20; published 2022 March 31

## Abstract

Some repeating fast radio burst (FRB) sources exhibit complex polarization behaviors, including frequency-dependent depolarization, variation of rotation measure (RM), and oscillating spectral structures of polarized components. Very recently, Feng et al. reported that active repeaters exhibit conspicuous frequency-dependent depolarization and a strong correlation between RM scatter ( $\sigma_{\text{RM}}$ ) and the temporal scattering time ( $\tau_s$ ),  $\sigma_{\text{RM}} \propto \tau_s^{1.0 \pm 0.2}$ , both of which can be well described by multipath propagation through a magnetized inhomogeneous plasma screen. This observation strongly suggests that the temporal scattering and RM scatter originate from the same region. Besides, a particular finding of note in Feng et al. is that the FRBs with compact persistent radio sources (PRSs) tend to have extreme  $\sigma_{\text{RM}}$ . In this work, we focus on some theoretical predictions of the relations among temporal scattering, depolarization by RM scatter, and PRSs contributed by the magnetized plasma environment close to a repeating FRB source. The behaviors of the RM scatter imply that the magnetized plasma environment is consistent with a supernova remnant or pulsar wind nebula, and the predicted  $\sigma_{\text{RM}}-\tau_s$  relation is  $\sigma_{\text{RM}} \propto \tau_s^{(0.54-0.83)}$  for different astrophysical scenarios. We further make a general discussion of PRSs that does not depend on specific astrophysical scenarios. We show that the specific luminosity of a PRS should have a positive correlation with the RM contributed by the plasma screen. This is consistent with the observations of FRB 121102 and FRB 190520B.

*Unified Astronomy Thesaurus concepts:* Compact radiation sources (678); Radio transient sources (2008); Radio bursts (1339); Radio continuum emission (1340); Interstellar medium (847)

## 1. Introduction

Fast radio bursts (FRBs) are cosmological radio transients with millisecond durations. Since the first FRB (FRB 010724, the Lorimer burst) was discovered in 2007 (Lorimer et al. 2007), hundreds of FRB sources have been detected, dozens of which are repeaters (e.g., the CHIME/FRB Collaboration et al. 2021). Recently, a Galactic FRB, FRB 200428, was detected to be associated with SGR J1935+2154 (Bochenek et al. 2020; CHIME/FRB Collaboration et al. 2020; Mereghetti et al. 2020; Li et al. 2021a; Ridnaia et al. 2021; Tavani et al. 2021), which suggests that at least some FRBs originate from magnetars born from the core collapse of massive stars (e.g., Popov & Postnov 2013; Katz 2016; Murase et al. 2016; Beloborodov 2017; Kumar et al. 2017; Yang & Zhang 2018, 2021; Metzger et al. 2019; Lu et al. 2020; Margalit et al. 2020; Wadiasingh et al. 2020; Wang et al. 2022; Zhang 2022). However, FRB 20200120E was found to be in a globular cluster of a nearby galaxy, M81 (Bhardwaj et al. 2021; Kirsten et al. 2022). This is in tension with the scenario that invokes active magnetars with ages  $\lesssim 10$  kyr formed in core-collapse supernovae (Kremer et al. 2021; Lu et al. 2022) and suggests that FRBs might originate from magnetars formed in compact binary mergers

(Margalit et al. 2019; Wang et al. 2020; Zhong et al. 2020; Zhao et al. 2021). Therefore, the physical origin of FRBs is still not well constrained from the data (e.g., Cordes & Chatterjee 2019; Petroff et al. 2019; Zhang 2020; Xiao et al. 2021). The growing FRB detections start to shed light on the diversity among the phenomena. The repeaters presented in the first CHIME FRB catalog have relatively larger widths and narrower bandwidths compared with one-off FRBs (Pleunis et al. 2021). The behaviors of fluence with respect to peak flux exhibit statistically significant differences between bursts with long and short durations (Li et al. 2021c). Multiple origins for the FRB population seem increasingly likely.

The first known repeater, FRB 121102, possesses numerous interesting properties, including (1) a bright persistent radio counterpart with a luminosity of  $\nu L_\nu \sim 10^{39} \text{ erg s}^{-1}$  at  $\nu \sim 10$  GHz that is spatially coincident with the FRB source (Chatterjee et al. 2017; Chen et al. 2022); (2) a large rotation measure (RM),  $|\text{RM}| \sim 10^5 \text{ rad m}^{-2}$  (Michilli et al. 2018), with a decreasing trend of evolution over a period of a few years (Hilmarsson et al. 2021a); (3) a large dispersion measure (DM) contribution ( $55 \text{ pc cm}^{-3} \lesssim \text{DM}_{\text{host}} \lesssim 225 \text{ pc cm}^{-3}$ ) from its host galaxy (Tendulkar et al. 2017); and (4) a high burst rate and bimodal energy distribution with time evolution (Li et al. 2021b). These properties imply that FRB 121102 has a magneto-ionic environment and an active central engine. When relativistic electrons hold a good proportion of the electron

population in a dense magnetized plasma, bright persistent radio emission is generated by synchrotron radiation (Murase et al. 2016; Kashiyama & Murase 2017; Metzger et al. 2017; Margalit & Metzger 2018; Yang et al. 2020).<sup>8</sup>

In addition to FRB 121102, some repeaters recently studied by the Five-hundred-meter Aperture Spherical radio Telescope (FAST; Li et al. 2019) also exhibit signs of complex magnetized plasma environments. First discovered through drift scans of the Commensal Radio Astronomy FAST Survey (Li et al. 2018), FRB 190520B (Niu et al. 2021) is colocated with a compact, persistent radio source (PRS) with a luminosity similar to that of FRB 121102, and its host is a dwarf galaxy at  $z = 0.241$  with a high specific star formation rate. The estimated DM contribution from the host is  $DM_{\text{host}} \simeq 900 \text{ pc cm}^{-3}$ , nearly an order of magnitude higher than those of other FRBs, which might be explained by a supernova remnant (e.g., Zhao & Wang 2021; Katz 2022).

Another active repeater, FRB 20201124A (Hilmarsson et al. 2021a; Kumar et al. 2022; Lanman et al. 2022; Nimmo et al. 2021), is found in a Milky Way-sized, metal-rich, barred-spiral host galaxy at  $z = 0.098$  (Fong et al. 2021; Piro et al. 2021; Ravi et al. 2021; Xu et al. 2021). This repeater indicates a significant, irregular variation of the Faraday rotation over 36 days. Some bursts appear to have circular polarization up to 75% (Hilmarsson et al. 2021b; Kumar et al. 2022; Xu et al. 2021). In particular, the frequency spectra of both the circular and linear polarization of some bursts with moderate circular polarization show clear oscillating structures (Xu et al. 2021), which might originate from the polarized absorption or the Faraday conversion mechanism (Melrose & Luo 2004; D. Li et al. 2022, in preparation).

On the other hand, turbulence generally exists in complex magnetized plasma environments, leading to temporal scattering, scintillation, depolarization, etc. The temporal scattering time of some FRBs is much longer than that of radio pulsars at high Galactic latitudes (Cordes et al. 2016). Meanwhile, the lack of any correlation between scattering time and the DM of FRBs implies that the intergalactic medium cannot account for both scattering time and DM,<sup>9</sup> and a detailed analysis of the turbulence effect of the intergalactic medium can be found in Beniamini & Kumar (2020). Qiu et al. (2020) studied the profiles of some FRBs detected by the Australian Square Kilometre Array Pathfinder. Five FRBs were identified with evidence of millisecond pulse broadening caused by scattering in an inhomogeneous plasma, and they suggested that the temporal scattering could be caused by the interstellar medium or near-source plasma in the host galaxy. Theoretically, Xu & Zhang (2016) examined some possible density fluctuation turbulence models and found that a shortwave-dominated power-law density spectrum can interpret the scattering timescale of FRBs. Simard & Ravi (2021) constrained the turbulence properties by comparing the measurements of FRB scattering with the optical recombination-line tracers of their host environments. In a cold magnetized or relativistic plasma, Faraday conversion could occur when an FRB propagates in the medium, leading to the conversion of linearly polarized emission

to circularly polarized emission (Gruzinov & Levin 2019; Vedantham & Ravi 2019). In a recent study, Beniamini et al. (2021) systematically studied the observed polarization properties of an FRB propagating in a magnetized plasma screen via multipath propagation.

More recently, Feng et al. (2022) reported new polarization measurements of five active repeaters, including FRB 121102, FRB 190520B, FRB 190303, FRB 190417, and FRB 20201124A, with FAST and the Green Bank Telescope. These bursts exhibit a conspicuous frequency-dependent linear polarization fraction that can be well described by RM scatter,  $\sigma_{\text{RM}}$  (see Section 2.2 for a detailed discussion about the depolarization by RM scatter). Furthermore, the scattering time  $\tau_s$  of these bursts shows a strong correlation with RM scatter,<sup>10</sup>  $\sigma_{\text{RM}} \propto \tau_s^{1.0 \pm 0.2}$ , which implies that  $\sigma_{\text{RM}}$  and  $\tau_s$  likely originate from the same environment.

In this work, we propose that temporal scattering, depolarization by RM scatter, and persistent radio emission all originate from the magnetized plasma environment near an FRB source and predict the relations among them. The paper is organized as follows. We consider that an FRB propagates in a magneto-ionic inhomogeneous plasma screen and calculate temporal scattering and depolarization by RM scatter in Section 2. The persistent radio emission from the magnetized plasma screen is analyzed in Section 3. The results are discussed and summarized in Section 4.

## 2. Temporal Scattering and Depolarization by RM Scatter from a Magnetized Plasma Screen

### 2.1. Temporal Scattering

We consider a power-law spectrum of electron density fluctuations in a magnetized plasma screen with thickness  $\Delta R$  satisfying

$$P(k) = C_N^2 k^{-\beta}, \quad \text{for } 2\pi L^{-1} \lesssim k \lesssim 2\pi l_0^{-1}, \quad (1)$$

where  $k = 2\pi/l$  is the spatial wavenumber;  $L$  and  $l_0$  are the outer and inner scales delineating the inertial range of the turbulence, respectively;  $\beta$  is the spectral index of the three-dimensional power spectrum; and Kolmogorov turbulence has  $\beta = 11/3$ . Using the normalization of the power spectrum  $\int P(\vec{k}) d\vec{k} = \delta n_{e,0}^2$ , one has (e.g., Xu & Zhang 2017)

$$C_N^2 \simeq \begin{cases} \frac{3 - \beta}{2(2\pi)^{4-\beta}} l_0^{3-\beta} \delta n_{e,0}^2, & \text{for } \beta < 3, \\ \frac{\beta - 3}{2(2\pi)^{4-\beta}} L^{3-\beta} \delta n_{e,0}^2, & \text{for } \beta > 3, \end{cases} \quad (2)$$

where  $\delta n_{e,0}^2$  is the total mean squared density fluctuation. According to Equation (1), for  $l_0 < l < L$ , the electron density

<sup>8</sup> See, however, Yang et al. (2016) and Li et al. (2020) for an alternative interpretation that the persistent radio emission might be generated by synchrotron heating of a synchrotron nebula by the radio bursts themselves.

<sup>9</sup> This is different from radio pulsars. For radio pulsars, a relation between scattering time and DM has been established (Cordes et al. 2016), which implies that the scattering time and DM are contributed by the same source.

<sup>10</sup> Notice that the relation in Figure 4 of Feng et al. (2022) is  $\tau_s \propto \sigma_{\text{RM}}^{0.81 \pm 0.16}$ , and the temporal scattering times of all FRBs have been scaled to  $\nu \sim 1.3$  GHz. For the same data, one has  $\sigma_{\text{RM}} \propto \tau_s^{1.03 \pm 0.21}$ .

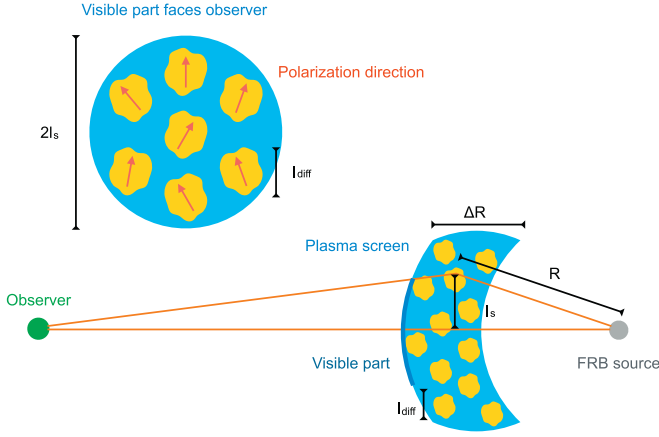


**Figure 1.** Schematic configuration of an FRB propagating in a magnetized inhomogeneous plasma screen. The yellow regions correspond to clumps with a diffractive length scale  $l_{\text{diff}}$ . The top left corner shows the polarization directions of electromagnetic waves from each clump, when the visible part of the plasma screen faces the observer.

fluctuation  $\delta n_{e,l}$  at scale  $l$  is

$$\delta n_{e,l}^2 \sim 4\pi C_N^2 k^{3-\beta} \sim \begin{cases} \delta n_{e,0}^2 \left(\frac{l}{l_0}\right)^{\beta-3}, & \text{for } \beta < 3, \\ \delta n_{e,0}^2 \left(\frac{l}{L}\right)^{\beta-3}, & \text{for } \beta > 3. \end{cases} \quad (3)$$

When the radio wave propagates in a turbulent medium, the fluctuating refractive indices introduce random phase fluctuations to the wave front, as shown in Figure 1. The “phase structure function” is used to represent the mean squared phase difference between two points separated by  $l$ ,  $D_\phi(\vec{l}) \equiv \langle [\phi(\vec{x} + \vec{l}) - \phi(\vec{x})]^2 \rangle$ . If the turbulence in the plasma screen is isotropic and  $L \ll \Delta R$ , the phase structure function is given by (Coles et al. 1987; Rickett 1990; Xu & Zhang 2017)

$$D_\phi(l) \simeq \begin{cases} f_{1,\alpha} \pi^2 r_e^2 \lambda^2 C_N^2 \Delta R l_0^{\beta-2} \left(\frac{l}{l_0}\right)^2, & \text{for } l \lesssim l_0, \\ f_{2,\alpha} \pi^2 r_e^2 \lambda^2 C_N^2 \Delta R l_0^{\beta-2} \left(\frac{l}{l_0}\right)^{\beta-2}, & \text{for } l \gtrsim l_0, \end{cases} \quad (4)$$

where  $\lambda$  is the wavelength of the electromagnetic wave,  $f_{1,\alpha} = \Gamma(1 - \alpha/2)$ ,  $f_{2,\alpha} = [\Gamma(1 - \alpha/2)/\Gamma(1 + \alpha/2)](8/\alpha 2^\alpha)$ , and  $\alpha = \beta - 2$ . For the Kolmogorov turbulence with  $\alpha = 5/3$  ( $\beta = 11/3$ ), one has  $f_{1,\alpha} = 5.6$  and  $f_{2,\alpha} = 8.9$ , respectively. We define  $l_{\text{diff}}$  as the diffractive length scale that represents the transverse separation for which the rms difference is equal to 1 rad, leading to  $D_\phi(l_{\text{diff}}) = 1$ , and one has

$$l_{\text{diff}} = \begin{cases} (f_{1,\alpha} \pi^2 r_e^2 \lambda^2 l_0^{\beta-4} C_N^2 \Delta R)^{-\frac{1}{2}}, & \text{for } l_{\text{diff}} < l_0, \\ (f_{2,\alpha} \pi^2 r_e^2 \lambda^2 C_N^2 \Delta R)^{\frac{1}{\beta-2}}, & \text{for } l_{\text{diff}} > l_0. \end{cases} \quad (5)$$

For the multipath propagation, as shown in Figure 1, the scattering angle of the electromagnetic waves is approximately  $\theta_s \simeq \lambda/2\pi l_{\text{diff}}$ . Therefore, the transverse scale of the visible part is

$$l_s(\lambda) = \theta_s R \simeq \frac{\lambda R}{2\pi l_{\text{diff}}}, \quad (6)$$

where  $R$  is the distance from the plasma screen to the source. The path-length difference between two rays is  $\Delta s \simeq R(1 - \cos \theta_s) \simeq R\theta_s^2/2$  for  $\theta_s \ll 1$ . The temporal scattering time could then be estimated by<sup>11</sup>

$$\tau_s(\lambda) \simeq \frac{l_s^2}{2Rc} = \frac{\lambda^2 R}{8\pi^2 c l_{\text{diff}}^2}. \quad (7)$$

Using Equation (5) and  $\Delta R \sim R$ , the temporal scattering time satisfies

$$\tau_s(\lambda) \propto \begin{cases} \delta n_{e,0}^2 R^2 \lambda^4, & l_{\text{diff}} < l_0, \\ \delta n_{e,0}^{\frac{4}{\beta-2}} R^{\frac{\beta}{\beta-2}} \lambda^{\frac{2\beta}{\beta-2}}, & l_{\text{diff}} > l_0. \end{cases} \quad (8)$$

For a certain plasma screen, scintillation and temporal scattering occur together and have a relation of  $\Delta\nu_{\text{sci}} = 1/(2\pi\tau_s)$ , where  $\Delta\nu_{\text{sci}}$  is the scintillation bandwidth. In general, scintillation refers to spectral modulations, and temporal scattering refers to temporal broadening of pulses due to the multipath propagation effect. The relation between scintillation and temporal scattering is due to the following: if the optical path difference is  $\sim c\tau_s$ , the phase difference is  $\sim (2\pi/\lambda)c\tau_s = 2\pi\nu\tau_s$ ; thus, the phase of the interference waves changes by  $\sim 1$  rad in the bandwidth of  $\Delta\nu_{\text{sci}} = 1/(2\pi\tau_s)$ . The value of  $\Delta\nu_{\text{sci}} \simeq 160 \text{ Hz}(\tau_s/1 \text{ ms})^{-1}$  is much smaller than the observed scintillation bandwidth of  $\sim 1$  MHz. This result suggests that for extragalactic FRBs, the observed scintillation is mainly contributed by the interstellar medium within the Milky Way, whereas the observed scattering time is more likely contributed by the circumburst medium or the interstellar medium in the FRB host galaxy.

## 2.2. Depolarization Due to RM Scatter

Next, we discuss the depolarization effect of the RM scatter from the magnetized plasma screen. This has been discussed by Beniamini et al. (2021), but here we show that there is a correlation between two measurable quantities, i.e., the scattering time and the depolarization wavelength, the critical wavelength below which radio waves are depolarized. We consider that there is a fluctuation in  $n_e$  and  $B_{\parallel}$  across the length scale  $l$ . In a magneto-ionic cold plasma, the dispersion relation of left and right circularly polarized waves is approximately

$$\frac{k^2 c^2}{\omega^2} \simeq 1 - \frac{\omega_p^2}{\omega^2} \pm \frac{\omega_p^2 \omega_B}{\omega^3} \quad (9)$$

for  $\omega \gg \omega_B$ , where  $\omega_p = (4\pi e^2 n_e / m_e)^{1/2}$  is the plasma frequency, and  $\omega_B = eB_{\parallel} / m_e c$  is the electron cyclotron frequency. Faraday rotation is related to the parallel component  $B_{\parallel} = B \cos \theta$ , and  $\theta$  is the angle between the wavevector and the local magnetic field. For a certain polarized wave (left or right circularly polarized waves) propagating in a homogeneous medium with scale  $l$ , the phase difference before and

<sup>11</sup> Notice that, due to the expansion of the universe, the observed wavelength is  $\lambda_{\text{obs}} = (1+z)\lambda$ , where  $\lambda$  is the wavelength at the plasma screen. Considering that most repeaters are at low redshifts, we ignore the redshift correction in the following discussion.

after crossing the medium is  $\phi_{\pm} = k_{\pm} l$  (apart from the trivial light travel time difference). A given path contains, on average,  $N = \Delta R/l$  independent segments, and the Poisson rms fluctuation is  $\Delta N = (\Delta R/l)^{1/2}$  in the limit of  $\Delta N \gg 1$ . Therefore, the total phase perturbation contributed by the plasma screen with an inhomogeneous medium is

$$\begin{aligned} \Delta\phi_{\pm}(l) &= \left(\frac{\Delta R}{l}\right)^{1/2} \delta\phi_{\pm} \\ &\simeq \left(\frac{\Delta R}{l}\right)^{1/2} \frac{\omega l}{c} \left[ \frac{\delta(\omega_p^2)}{2\omega^2} \mp \frac{\delta(\omega_p^2 \omega_B)}{2\omega^3} \right] \end{aligned} \quad (10)$$

for  $\omega \gg \omega_B, \omega_p$ , where  $\delta\phi_{\pm}$  is the phase perturbation of the left/right circularly polarized waves in a clump with length scale  $l$ . The perturbation of the Faraday rotation angle after a radio burst propagating across the plasma screen is  $\Delta\psi = |\Delta\phi_{+} - \Delta\phi_{-}|/2$ , i.e.,

$$\Delta\psi(l) \simeq \left(\frac{\Delta R}{l}\right)^{1/2} \delta\text{RM}(l) \lambda^2 = \frac{2\pi e^3 (l\Delta R)^{1/2}}{m_e^2 c^2 \omega^2} \delta(n_e B_{\parallel})_l, \quad (11)$$

where the RM contribution by a clump with scale  $l$  is given by

$$\delta\text{RM}(l) = \frac{e^3}{2\pi m_e^2 c^4} \delta(n_e B_{\parallel})_l, \quad (12)$$

and  $\delta(n_e B_{\parallel})_l$  is on the scale of  $l$ . One must notice that the decorrelation length scale of the Faraday rotation angle is different from the diffractive scale  $l_{\text{diff}}$  that reflects the phase structure function, as shown in Figure 1.

Since the rotation angle  $\Delta\psi$  increases with  $l$ , the most important contribution comes from the largest transverse separation  $l_s$  given by Equation (6). Let us consider the source to be 100% linearly polarized. If  $\Delta\psi(l_s) \gg 1$  rad, the observed waves at any given time will be the superposition of a large number of patches with random polarization directions. The size of each patch,  $l_{\text{PA}}$ , can be estimated by<sup>12</sup>  $\Delta\psi(l_{\text{PA}}) \sim 1$  rad. Then, when we add up the contributions from many  $l_{\text{PA}}$  patches, the final waves are unpolarized. Therefore, depolarization occurs at the depolarization wavelength  $\lambda_{\text{dep}}$  when  $\Delta\psi(l_s) \sim 1$  rad. The RM scatter contributed by the plasma screen is estimated by

$$\begin{aligned} \sigma_{\text{RM}} &\simeq \left(\frac{\Delta R}{l_s}\right)^{1/2} \delta\text{RM}(l_s) \\ &= \frac{e^3}{2\pi m_e^2 c^4} (l_s \Delta R)^{1/2} \delta(n_e B_{\parallel})_{l_s} \\ &= 0.81 \text{ rad m}^{-2} \left( \frac{\sqrt{l_s \Delta R}}{1 \text{ pc}} \right) \left( \frac{\delta(n_e B_{\parallel})_{l_s}}{1 \text{ cm}^{-3} \mu\text{G}} \right), \end{aligned} \quad (13)$$

and the depolarization wavelength is

$$\lambda_{\text{dep}} \sim \sigma_{\text{RM}}^{-1/2}. \quad (14)$$

<sup>12</sup> We consider the realistic limit  $\omega_B \ll \omega$  (or  $B \ll 1$  kG for a gigahertz wave) and hence  $\Delta\psi(l) \ll \Delta\phi(l)$ . Thus, each patch of the size of  $l_{\text{PA}}$  contains many subpatches (each of the size of  $l_{\text{diff}}$ ) of different phases, and even though the waves contributed by a patch of  $l_{\text{PA}}$  have the same polarization direction, the phase coherence is lost.

We notice that the observed RM scatter  $\sigma_{\text{RM}}$  should always be less than the absolute value of RM contributed by the magnetized plasma screen. The observed result of  $\sigma_{\text{RM}} \ll |\text{RM}|$  (Feng et al. 2022) implies that a large-scale magnetic field may exist in the screen, or the observed RM is contributed by other regions. According to Equations (7) and (13), eliminating  $l_s$  and taking  $\Delta R \sim R$ , one finally obtains

$$\begin{aligned} \sigma_{\text{RM}} &\simeq \frac{e^3}{2\pi m_e^2 c^4} \delta(n_e B_{\parallel})_{l_s} (2R^3 c \tau_s(\lambda_{\text{dep}}))^{1/4} = 1.7 \text{ rad m}^{-2} \\ &\times \left(\frac{R}{1 \text{ pc}}\right)^{3/4} \left(\frac{\delta(n_e B_{\parallel})_{l_s}}{10^3 \text{ cm}^{-3} \mu\text{G}}\right) \left(\frac{\tau_s(\lambda_{\text{dep}})}{1 \text{ ms}}\right)^{1/4}, \end{aligned} \quad (15)$$

where  $\tau_s(\lambda_{\text{dep}})$  is the scattering time at the depolarization wavelength. Some repeating FRBs studied by Feng et al. (2022) have RM scatter values  $\sigma_{\text{RM}} \gtrsim 1 \text{ rad m}^{-2}$ . This is consistent with the picture that the RM scatter and temporal scattering originate from radio bursts propagating in an inhomogeneous magneto-ionic environment near the source. The above typical parameters of the plasma screen are consistent with the scenario of a supernova remnant or pulsar wind nebula (Reynolds et al. 2012; Feng et al. 2022).

### 2.3. $\sigma_{\text{RM}}-\tau_s$ Relations

In order to obtain the  $\sigma_{\text{RM}}-\tau_s$  relation, we would like to relate  $\sigma_{\text{RM}}$  to the temporal scattering time  $\tau_{s,0}$  at a fixed wavelength  $\lambda_0$  for all repeaters, as measured by Feng et al. (2022). According to Equations (8) and (14), the temporal scattering time at wavelength  $\lambda_{\text{dep}}$  is given by

$$\tau_s \propto \begin{cases} \sigma_{\text{RM}}^{-2} \tau_{s,0}, & l_{\text{diff}} < l_0, \\ \sigma_{\text{RM}}^{\frac{\beta}{2-\beta}} \tau_{s,0}, & l_{\text{diff}} > l_0. \end{cases} \quad (16)$$

Since the length scale of the visible part,  $l_s$ , could be larger than the maximum length scale  $L$  of the turbulence, we will discuss the cases of  $l_s \lesssim L$  and  $l_s \gtrsim L$ .

(1)  $l_0 \lesssim l_s \lesssim L$ . In this case, one has  $\delta n_e \ll n_e$  and  $\delta B_{\parallel} \ll B_{\parallel}$ , so that

$$\delta(n_e B_{\parallel}) \sim B_{\parallel} \delta n_e. \quad (17)$$

Using Equations (3) and (7), one further obtains  $\delta(n_e B_{\parallel})_{l_s} \propto B_{\parallel} \delta n_{e,0} l_s^{(\beta-3)/2} \propto B_{\parallel} \delta n_{e,0} \tau_s^{(\beta-3)/4} R^{(\beta-3)/4}$ . Using Equation (16), one gets

$$\delta(n_e B_{\parallel})_{l_s} \propto \begin{cases} B_{\parallel} \delta n_{e,0} \sigma_{\text{RM}}^{\frac{3-\beta}{2}} \tau_{s,0}^{\frac{\beta-3}{4}} R^{\frac{\beta-3}{4}}, & l_{\text{diff}} < l_0, \\ B_{\parallel} \delta n_{e,0} \sigma_{\text{RM}}^{\frac{\beta(\beta-3)}{4(2-\beta)}} \tau_{s,0}^{\frac{\beta-3}{4}} R^{\frac{\beta-3}{4}}, & l_{\text{diff}} > l_0. \end{cases} \quad (18)$$

According to Equations (8), (15), (16), and (18), one finally obtains the  $\sigma_{\text{RM}}-\tau_{s,0}$  relation,

$$\sigma_{\text{RM}} \propto \begin{cases} \tau_{s,0}^{\frac{1}{2}} R^{\frac{\beta-4}{2\beta}} B_{\parallel}^{\frac{2}{\beta}}, & l_{\text{diff}} < l_0, \\ \tau_{s,0}^{\frac{2(\beta-2)}{\beta+4}} R^0 B_{\parallel}^{\frac{4}{\beta+4}}, & l_{\text{diff}} > l_0. \end{cases} \quad (19)$$

(2)  $l_s \gtrsim L$ . In this case, one has  $\delta n_e \sim \delta n_{e,0} \sim n_e$  and  $\delta B_{\parallel} \sim \delta B_{\parallel,0} \propto B_{\parallel}$ , where  $\delta B_{\parallel,0}$  is the total rms parallel magnetic field. For the global turbulent magnetic field,  $\delta B_{\parallel,0} \sim B_{\parallel}$ . For



the magnetic field with turbulent and large-scale components,  $\delta B_{\parallel,0} < B_{\parallel}$ . Thus, one may have

$$\delta(n_e B_{\parallel})_{l_s} \propto B_{\parallel} \delta n_{e,0}. \quad (20)$$

Using Equations (8), (15), (16), and (20), the  $\sigma_{\text{RM}}-\tau_{s,0}$  relation becomes

$$\sigma_{\text{RM}} \propto \begin{cases} \tau_{s,0}^{\frac{1}{2}} R^{-\frac{1}{6}} B_{\parallel}^{\frac{2}{3}}, & l_{\text{diff}} < l_0, \\ \tau_{s,0}^{\frac{(\beta-2)(\beta-1)}{5\beta-8}} R^{\frac{\beta^2-5\beta+6}{8-5\beta}} B_{\parallel}^{\frac{4(\beta-2)}{5\beta-8}}, & l_{\text{diff}} > l_0. \end{cases} \quad (21)$$

The  $\sigma_{\text{RM}}-\tau_s$  relation given by Equations (19) and (21) involves several parameters connected to the nature of the screens, including screen radius  $R$ , line-of-sight component of the magnetic field  $B_{\parallel}$ , turbulence inner scale  $l_0$ , etc., which may vary between different FRBs, and the variations of these parameters would affect the scatter of the  $\sigma_{\text{RM}}-\tau_s$  relation. The larger the variation of these parameters, the larger the scatter of the  $\sigma_{\text{RM}}-\tau_s$  relation. Furthermore, the dependence on distance  $R$  is negligible, and the only unknown is  $B_{\parallel}$ . Because the sources with stronger turbulent fluctuations are expected to have a higher magnetic field strength, we expect the scaling to be steeper than  $\sigma_{\text{RM}} \propto \tau_{s,0}^{1/2}$ .

In the following, we propose to estimate the parallel component of the magnetic field by the fluctuations of RM and DM (Katz 2018, 2021),

$$\begin{aligned} B_{\parallel} &\simeq \frac{2\pi m_e^2 c^4}{e^3} \frac{\Delta \text{RM}}{\Delta \text{DM}} \\ &= 1.2 \text{ mG} \left( \frac{\Delta \text{RM}}{10^3 \text{ rad m}^{-2}} \right) \left( \frac{\Delta \text{DM}}{1 \text{ pc cm}^{-3}} \right)^{-1}. \end{aligned} \quad (22)$$

Because the large-scale plasma, e.g., the interstellar or intergalactic medium, contributes to nearly time-invariant RM and DM, the fluctuations  $\Delta \text{RM}$  and  $\Delta \text{DM}$  on timescales less than a few years are expected to originate from either the time evolution of the local plasma or the proper motion of the source with respect to the local plasma (Yang & Zhang 2017; Piro & Gaensler 2018).

If one conducts an extensive monitoring campaign on a repeater source, it is possible to measure the rms variation of  $\langle \Delta \text{RM} \rangle_t$  and  $\langle \Delta \text{DM} \rangle_t$ , where  $\langle \dots \rangle_t$  denotes an ensemble average of multiple measurements of different  $\Delta \text{RM}$  and  $\Delta \text{DM}$  at a time separation of  $t$ . For example, FRB 121102 had an average increase of DM of  $\sim 1 \text{ pc cm}^{-3} \text{ yr}^{-1}$  (Hessels et al. 2019) and an average decrease of RM of  $\sim 10^4 \text{ rad m}^{-2} \text{ yr}^{-1}$  (Hilmarsson et al. 2021a), so we infer  $B_{\parallel} \sim 10 \text{ mG}$ . Another source, FRB 20201124A, had strong RM fluctuations of  $\Delta \text{RM} \sim 200 \text{ rad m}^{-2}$  on a timescale of 10 days (Xu et al. 2021), whereas its DM fluctuation is not well measured (due to the long scattering time) but constrained to be  $\Delta \text{DM} \lesssim 3 \text{ pc cm}^{-3}$  on a similar timescale (Xu et al. 2021). For this source, we can infer  $B_{\parallel} \gtrsim 0.1 \text{ mG}$ . Even if good measurements of  $\Delta \text{RM}$  and  $\Delta \text{DM}$  are not available, for a source with a large RM  $\gtrsim 500 \text{ rad m}^{-2}$ , the main contributor to RM would possibly be from the local plasma. Meanwhile, the upper limit on the local DM may be inferred from the host galaxy redshift and Galactic DM contributions, so it is still possible to estimate a lower limit of  $B_{\parallel}$  in the local plasma. Therefore, the relations of Equations (19) and (21) can be tested by observations.

Since the magnetic fields near most repeaters have not been measured by the above method, in the following, we consider that the magnetic field–density relation satisfies

$$B = A n_e^{\kappa}. \quad (23)$$

Different sources have the same  $\kappa$  but different values of  $A$ . One may consider two cases. (1) If  $l_0 \lesssim l_s \lesssim L$ , according to Equations (8) and (19), one obtains

$$\sigma_{\text{RM}} \propto \begin{cases} \tau_{s,0}^{\frac{\beta+2\kappa}{2\beta}} R^{\frac{\beta-4\kappa-4}{2\beta}}, & l_{\text{diff}} < l_0, \\ \tau_{s,0}^{\frac{(\beta-2)(\kappa+2)}{\beta+4}} R^{\frac{-\beta\kappa}{\beta+4}}, & l_{\text{diff}} > l_0. \end{cases} \quad (24)$$

We define the variation range of  $A$  for different sources as  $\delta A$ ; using Equation (19), the scatter contributed by  $\delta A$  of the above relation is

$$\frac{\delta \sigma_{\text{RM}}}{\bar{\sigma}_{\text{RM}}} = \begin{cases} \left( \frac{\delta A}{\bar{A}} \right)^{\frac{2}{\beta}}, & l_{\text{diff}} < l_0, \\ \left( \frac{\delta A}{\bar{A}} \right)^{\frac{4}{\beta+4}}, & l_{\text{diff}} > l_0. \end{cases} \quad (25)$$

(2) If  $l_s \gtrsim L$ , according to Equations (8) and (21), one obtains

$$\sigma_{\text{RM}} \propto \begin{cases} \tau_{s,0}^{\frac{2\kappa+3}{6}} R^{\frac{-(4\kappa+1)}{6}}, & l_{\text{diff}} < l_0, \\ \tau_{s,0}^{\frac{(\beta-2)(\kappa\beta+\beta-2\kappa-1)}{5\beta-8}} R^{\frac{(\kappa+1)\beta^2-(2\kappa+5)\beta+6}{8-5\beta}}, & l_{\text{diff}} > l_0. \end{cases} \quad (26)$$

Using Equation (21), the scatter of the above relation is

$$\frac{\delta \sigma_{\text{RM}}}{\bar{\sigma}_{\text{RM}}} = \begin{cases} \left( \frac{\delta A}{\bar{A}} \right)^{\frac{2}{3}}, & l_{\text{diff}} < l_0, \\ \left( \frac{\delta A}{\bar{A}} \right)^{\frac{4(\beta-2)}{5\beta-8}}, & l_{\text{diff}} > l_0. \end{cases} \quad (27)$$

In the following, we will discuss three different astrophysical scenarios.

### 2.3.1. Magnetized Plasma with Energy Equipartition

If the magnetized plasma screen roughly satisfies the energy equipartition between the magnetic and kinetic energy of thermal electrons, one has

$$n_e k_B T \sim \frac{B^2}{8\pi}, \quad (28)$$

where  $k_B$  is the Boltzmann constant, and  $T$  is the plasma temperature. (1) If  $l_0 \lesssim l_s \lesssim L$ , according to Equation (24), one obtains

$$\sigma_{\text{RM}} \propto \begin{cases} \tau_{s,0}^{\frac{\beta+1}{2\beta}} R^{\frac{\beta-6}{2\beta}}, & l_{\text{diff}} < l_0, \\ \tau_{s,0}^{\frac{5(\beta-2)}{2(\beta+4)}} R^{\frac{-\beta}{2(\beta+4)}}, & l_{\text{diff}} > l_0. \end{cases} \quad (29)$$

(2) If  $l_s \gtrsim L$ , according to Equation (26), one obtains

$$\sigma_{\text{RM}} \propto \begin{cases} \tau_{s,0}^{\frac{2}{3}} R^{-\frac{1}{2}}, & l_{\text{diff}} < l_0, \\ \tau_{s,0}^{\frac{(\beta-2)(3\beta-4)}{2(5\beta-8)}} R^{\frac{3(\beta-2)^2}{2(8-5\beta)}}, & l_{\text{diff}} > l_0. \end{cases} \quad (30)$$

This predicts  $\sigma_{\text{RM}} \propto \tau_{s,0}^{(0.54-0.67)}$  for Kolmogorov turbulence with  $\beta = 11/3$ , which is shallower than the observed relation

given by Feng et al. (2022). In particular, if the magnetized plasma screen is photoionized with a typical temperature of  $T \sim 10^4$  K, the scatter of the above relations would be very small.

### 2.3.2. Magnetic Freezing Plasma

We next consider that turbulent plasma satisfies the magnetic frozen condition, which might be satisfied when the magnetic reconnection is not significant. Then, one obtains

$$B = An_e^{2/3}. \quad (31)$$

(1) If  $l_0 \lesssim l_s \lesssim L$ , according to Equation (24), one obtains

$$\sigma_{\text{RM}} \propto \begin{cases} \tau_{s,0}^{\frac{3\beta+4}{6\beta}} R^{\frac{3\beta-20}{6\beta}}, & l_{\text{diff}} < l_0, \\ \tau_{s,0}^{\frac{8(\beta-2)}{3(\beta+4)}} R^{\frac{-2\beta}{3(\beta+4)}}, & l_{\text{diff}} > l_0. \end{cases} \quad (32)$$

(2) If  $l_s \gtrsim L$ , according to Equation (26), one obtains

$$\sigma_{\text{RM}} \propto \begin{cases} \tau_{s,0}^{\frac{13}{18}} R^{-\frac{11}{18}}, & l_{\text{diff}} < l_0, \\ \tau_{s,0}^{\frac{(\beta-2)(5\beta-7)}{3(5\beta-8)}} R^{\frac{5\beta^2-19\beta+18}{3(8-5\beta)}}, & l_{\text{diff}} > l_0. \end{cases} \quad (33)$$

This predicts  $\sigma_{\text{RM}} \propto \tau_{s,0}^{(0.58-0.72)}$  for Kolmogorov turbulence with  $\beta = 11/3$ . The scatters of the above relations depend on the range of  $A$  in the special astrophysical environments; see Equations (25) and (27).

### 2.3.3. Shock-compressed Magnetized Plasma

We further consider the case that the magnetized turbulent plasma is from a shocked medium and assume the interstellar medium as the upstream of the shocks. The Rankine–Hugoniot relation for a nonrelativistic perpendicular shock requires<sup>13</sup>

$$\frac{B}{n_e} \sim \left( \frac{B}{n_e} \right)_{\text{ISM}}. \quad (34)$$

Again according to Equations (24) and (26), we consider two cases. (1) If  $l_0 \lesssim l_s \lesssim L$ , one obtains

$$\sigma_{\text{RM}} \propto \begin{cases} \tau_{s,0}^{\frac{\beta+2}{2\beta}} R^{\frac{\beta-8}{2\beta}}, & l_{\text{diff}} < l_0, \\ \tau_{s,0}^{\frac{3(\beta-2)}{\beta+4}} R^{\frac{-\beta}{\beta+4}}, & l_{\text{diff}} > l_0. \end{cases} \quad (35)$$

(2) If  $l_s \gtrsim L$ , one obtains

$$\sigma_{\text{RM}} \propto \begin{cases} \tau_{s,0}^{\frac{5}{6}} R^{-\frac{5}{6}}, & l_{\text{diff}} < l_0, \\ \tau_{s,0}^{\frac{2\beta-3(\beta-2)}{5\beta-8}} R^{\frac{2\beta^2-7\beta+6}{8-5\beta}}, & l_{\text{diff}} > l_0. \end{cases} \quad (36)$$

This predicts  $\sigma_{\text{RM}} \propto \tau_{s,0}^{(0.65-0.83)}$  for Kolmogorov turbulence with  $\beta = 11/3$ . This theoretically predicted relation is closer to the observed relation (Feng et al. 2022) than the prediction of the model invoking magnetized turbulent plasma with energy equipartition or a magnetic frozen condition, as discussed in Sections 2.3.1 and 2.3.2, respectively. At last, we discuss the scatters of the above relations. In general, the interstellar medium satisfies the energy equipartition condition; thus, one

has  $A = B_{\text{ISM}}/n_{\text{ISM}} \propto n_{\text{ISM}}^{-1/2}$ . We assume that different FRB sources have  $n_{\text{ISM}}$  varying with 3 orders of magnitude; then,  $\delta A/\bar{A}$  varies with 1–2 orders of magnitude. According to Equations (25) and (27), the relative uncertainty  $\delta\sigma_{\text{RM}}/\bar{\sigma}_{\text{RM}}$  is with 1 order of magnitude, which is approximately consistent with the scatter of the observed relation (see Figure 4 of Feng et al. 2022).

## 3. Persistent Radio Emission from a Magnetized Plasma Screen

The FRB sources with large RM and  $\sigma_{\text{RM}}$  values imply a dense and magnetized environment, which could produce synchrotron radiation if relativistic electrons make up a significant fraction of the plasma energy density, powering a bright PRS (e.g., Murase et al. 2016; Metzger et al. 2017; Margalit & Metzger 2018; Yang et al. 2020). We consider that the electron distribution has a thermal component satisfying three-dimensional Maxwell distribution in the low-energy regime and a nonthermal component in the high-energy regime,<sup>14</sup> i.e.,

$$n_e(u) \equiv \frac{dn_e}{du} \simeq \begin{cases} \frac{n_e}{u_{\text{th}}} \left( \frac{u}{u_{\text{th}}} \right)^2, & u < u_{\text{th}}, \\ \frac{n_e}{u_{\text{th}}} \left( \frac{u}{u_{\text{th}}} \right)^{-p}, & u > u_{\text{th}}, \end{cases} \quad (37)$$

where  $u = \sqrt{\gamma^2 - 1}$  is the dimensionless four velocity,  $u_{\text{th}} = \sqrt{\gamma_{\text{th}}^2 - 1}$  is the thermal four velocity with  $\gamma_{\text{th}} = kT/m_e c^2 + 1$  as the thermal Lorentz factor, and  $p$  is the distribution index of the power-law component. The RM contribution from relativistic electrons is suppressed by a factor of  $\gamma^2$  due to the relativistic mass  $m_e \rightarrow \gamma m_e$ . Therefore, the RM contributed by the plasma screen with the above electron distribution is approximately given by (e.g., the Appendix of Quataert & Gruzinov 2000)

$$\text{RM} \simeq \frac{e^3}{2\pi m_e^2 c^4} \frac{n_e B_{\parallel}}{\gamma_{\text{th}}^2} \Delta R. \quad (38)$$

If the thermal component is nonrelativistic, i.e.,  $\gamma_{\text{th}} \sim 1$ , the RM would be mainly contributed by the nonrelativistic electrons, leading to the classical results.

For a single electron, the synchrotron radiation power is  $P = (4/3)\sigma_{\text{T}} c \gamma^2 B^2 / 8\pi$ , and the characteristic synchrotron frequency is  $\nu = \gamma^2 e B / 2\pi m_e c$ . Thus, the spectral radiation power satisfies  $P_{\nu} \simeq P/\nu = m_e c^2 \sigma_{\text{T}} B / 3e$ , which depends on  $B$  only. We define  $\zeta_e$  as the fraction of electrons that radiate synchrotron emission in the gigahertz band. The electrons emitting synchrotron radiation in the gigahertz band are required to have a Lorentz factor

$$\gamma_{\text{GHz}} \sim \left( \frac{2\pi m_e c \nu}{eB} \right)^{1/2} \simeq 600 \left( \frac{\nu}{1 \text{ GHz}} \right)^{1/2} \left( \frac{B}{1 \text{ mG}} \right)^{-1/2}; \quad (39)$$

<sup>13</sup> Notice that the shock surface may not necessarily be perpendicular to the line of sight. This may lead to a significant contribution of  $B_{\parallel}$ .

<sup>14</sup> The distribution given by Equation (37) is consistent with the particle-in-cell simulations of particle acceleration in relativistic shock (Spitkovsky 2008). However, one should notice that the Maxwell distribution in Spitkovsky (2008) is two-dimensional, leading to  $n_e(\gamma) \propto \gamma$  for  $\gamma \lesssim \gamma_{\text{th}}$ . For the three-dimensional Maxwell distribution, one has  $n_e(\gamma) \propto \gamma^2$  for  $\gamma \lesssim \gamma_{\text{th}}$  (Rybicki & Lightman 1979; Kato 2007).

then, the fraction  $\zeta_e$  is approximately given by

$$\zeta_e \sim \frac{\gamma_{\text{GHz}} n_e(\gamma_{\text{GHz}})}{n_e} \sim \left( \frac{\gamma_{\text{GHz}}}{\gamma_{\text{th}}} \right)^{1-p} \quad (40)$$

for  $\gamma_{\text{GHz}} > \gamma_{\text{th}}$ . The total number of relativistic electrons is approximately  $N_e \sim 4\pi R^2 \Delta R \zeta_e n_e / 3$  for  $\Delta R \sim R$ . The specific luminosity of the synchrotron radiation is

$$\begin{aligned} L_\nu &= N_e P_\nu = \frac{64\pi^3}{27} \zeta_e \gamma_{\text{th}}^2 m_e c^2 R^2 |\text{RM}| \\ &\simeq 5.7 \times 10^{29} \text{ erg s}^{-1} \text{ Hz}^{-1} \\ &\times \left( \frac{\zeta_e \gamma_{\text{th}}^2}{0.01} \right) \left( \frac{|\text{RM}|}{10^3 \text{ rad m}^{-2}} \right) \left( \frac{R}{1 \text{ pc}} \right)^2. \end{aligned} \quad (41)$$

Since  $p \sim 2$  is satisfied in most astrophysical scenarios of particle acceleration, one has  $\zeta_e \gamma_{\text{th}}^2 \sim \gamma_{\text{th}}^3 \gamma_{\text{GHz}}^{-1}$ . Therefore, according to Equation (39), a small value of  $\zeta_e \gamma_{\text{th}}^2$  requires  $\gamma_{\text{th}} \lesssim$  a few, and the thermal component could be nonrelativistic. At last, we are also interested in the specific luminosity related to  $\sigma_{\text{RM}}$ . We define  $\xi_{nB} = \delta(n_e B_{\parallel})_s / (n_e B_{\parallel})$  and  $\eta_l = (l_s / \Delta R)^{1/2}$ . According to Equations (13) and (38), the specific luminosity of the synchrotron radiation is

$$\begin{aligned} L_\nu &= \frac{64\pi^3}{27} \frac{\zeta_e \gamma_{\text{th}}^2}{\xi_{nB} \eta_l} m_e c^2 R^2 \sigma_{\text{RM}} \\ &\simeq 5.7 \times 10^{29} \text{ erg s}^{-1} \text{ Hz}^{-1} \left( \frac{\xi_{nB}}{0.1} \right)^{-1} \left( \frac{\eta_l}{0.1} \right)^{-1} \\ &\times \left( \frac{\zeta_e \gamma_{\text{th}}^2}{0.01} \right) \left( \frac{\sigma_{\text{RM}}}{10 \text{ rad m}^{-2}} \right) \left( \frac{R}{1 \text{ pc}} \right)^2. \end{aligned} \quad (42)$$

The results of Equations (41) and (42) suggest that FRBs with large RM and  $\sigma_{\text{RM}}$  values tend to be associated with compact PRSs. This is consistent with the observations of FRB 121102 and FRB 190520B (Yang et al. 2020; Feng et al. 2022).

Another way to estimate the radio luminosity is to assume that electrons radiating in the gigahertz band contribute a fraction of the total pressure so that it may scale with the magnetic pressure, i.e.,  $\gamma^2 (dn_e / d\gamma) m_e c^2 \sim B^2 / 8\pi$ . Because the electron distribution satisfies  $n_e(\gamma) \propto \gamma^{-2}$  in most astrophysical scenarios,  $\gamma^2 (dn_e / d\gamma)$  is roughly independent of  $\gamma$ . According to Equation (39), the specific luminosity is given by

$$\begin{aligned} L_\nu &\simeq \gamma \frac{dn_e}{d\gamma} \left( \frac{4\pi}{3} R^3 \right) P_\nu \simeq 3.7 \times 10^{27} \text{ erg s}^{-1} \text{ Hz}^{-1} \\ &\times \left( \frac{\nu}{1 \text{ GHz}} \right)^{-1/2} \left( \frac{B}{1 \text{ mG}} \right)^{7/2} \left( \frac{R}{1 \text{ pc}} \right)^3. \end{aligned} \quad (43)$$

If we further assume that the magnetic energy in the magnetized plasma screen is contributed by the central neutron star engine with a magnetic energy  $E_B$ , i.e.,  $(B^2 / 8\pi)(4\pi R^3 / 3) \sim \beta_B E_B$  with  $\beta_B < 1$ , then the above equation could be written as

$$\begin{aligned} L_\nu &\simeq 2.4 \times 10^{28} \text{ erg s}^{-1} \text{ Hz}^{-1} \eta_B \\ &\times \left( \frac{\nu}{1 \text{ GHz}} \right)^{-1/2} \left( \frac{B}{10 \text{ mG}} \right)^{3/2} \left( \frac{E_B}{10^{48} \text{ erg}} \right). \end{aligned} \quad (44)$$

This shows that the PRS should only be detected from sources with a strongly magnetized environment, e.g.,  $B \gtrsim 10$  mG. As the nebula expands with time, the magnetic energy drops due to adiabatic losses, and the magnetic field strength also decreases due to increasing volume; thus, one may only expect to detect bright PRSs from very young systems.

#### 4. Conclusions and Discussions

Recently, some newly discovered repeating FRBs were found to possess complex polarization properties and be associated with compact PRSs. For example, FRB 121102 showed a significant RM evolution during a long term (Michilli et al. 2018; Hilmarsson et al. 2021a); meanwhile, it was associated with a compact PRS (Chatterjee et al. 2017). The FRB 180301 exhibited significant polarization angle swings on a timescale of  $\sim 10$  ms while maintaining a large polarization degree (Luo et al. 2020). The FRB 190520B was also found to be associated with a compact PRS and have an extremely significant DM contribution by its host galaxy (Niu et al. 2021). The FRB 20201124A showed significant, irregular, short-time variation of the Faraday rotation, and the frequency spectra of the polarized components of some bursts appear to show clear oscillating structures (Xu et al. 2021). Very recently, Feng et al. (2022) reported that active repeaters exhibit conspicuous frequency-dependent depolarization and a strong correlation between  $\sigma_{\text{RM}}$  and  $\tau_s$  ( $\sigma_{\text{RM}} \propto \tau_s^{1.0 \pm 0.2}$ ); meanwhile, the FRBs with compact PRSs tend to have extreme RM scatter. The observational properties imply that these FRB sources are located in magnetized plasma environments, likely a supernova remnant or pulsar wind nebula.






Theories on the temporal scattering and depolarization of FRBs have been discussed in previous works (e.g., Xu & Zhang 2016; Beniamini & Kumar 2020; Beniamini et al. 2021). In this work, we mainly focus on some theoretical predictions of the relations among temporal scattering, depolarization by RM scatter, and persistent radio emission contributed by the magnetized plasma environment close to a repeating FRB source. First, we predict a relation between RM scatter and temporal scattering time, as shown by Equations (19) and (21). Since  $B_{\parallel} \propto \Delta \text{RM} / \Delta \text{DM}$  is involved (Katz 2018, 2021), such a relation could be tested once the rms variations of DM and RM are measured for repeating FRBs in the future. Furthermore, if one assumes that the turbulent plasma satisfies energy equipartition with  $B \propto n_e^{1/2}$ , then the relation between RM scatter and temporal scattering time becomes Equations (29) and (30), which gives  $\sigma_{\text{RM}} \propto \tau_{s,0}^{(0.54-0.67)}$  for the Kolmogorov turbulence. This is shallower than the observed relation by Feng et al. (2022). If the turbulent plasma satisfies the magnetic frozen condition with  $B \propto n_e^{2/3}$ , the predicted  $\sigma_{\text{RM}} - \tau_s$  becomes Equations (32) and (33), which gives  $\sigma_{\text{RM}} \propto \tau_s^{(0.58-0.72)}$  for the Kolmogorov turbulence. If the turbulent plasma is shock compressed with  $B \propto n_e$ , the predicted  $\sigma_{\text{RM}} - \tau_s$  becomes Equations (35) and (36), which gives  $\sigma_{\text{RM}} \propto \tau_s^{(0.65-0.83)}$  for the Kolmogorov turbulence. This is closer to the observed relation (Feng et al. 2022). Besides, since the RM scatters measured by the frequency-dependent depolarization are much less than the absolute values of the RMs of most repeaters (Feng et al. 2022), it implies that a large-scale magnetic field may exist in the plasma screen, or the observed RM is from a different region. Very recently, Anna-Thomas et al. (2022) reported that the RM of FRB 190520B is rapidly varying with a

large amplitude. Since the  $\sigma_{\text{RM}}$  affecting the depolarization is mainly contributed by the small-scale fluctuation  $\delta(n_e B_{\parallel})$  with a scale much less than  $l_s$  given by Equation (6), the result of  $|\text{RM}| \gg \sigma_{\text{RM}}$  implies that the observed varying RM is mainly contributed by the large-scale magnetic field, and  $\delta B \ll B$  is required.

We then discuss the relation between RM and the luminosity of the PRS for repeating FRBs. Different from most previous works with PRSs depending on some specific astrophysical scenarios (e.g., Yang et al. 2016; Dai et al. 2017; Margalit & Metzger 2018), in this work, we make a general discussion, only assuming that PRSs and RM originate from the same region and PRSs are produced by synchrotron radiation. We find that the thermal component of accelerated electrons could not be ultrarelativistic. We also predict that the larger the RM and/or RM scatter, the brighter the persistent radio emission from the plasma screen. This result is consistent with the observation of FRB 121102 (Chatterjee et al. 2017; Michilli et al. 2018; Yang et al. 2020). According to this picture, FRB 190520B with a compact PRS should also have a relatively large RM value. This is consistent with the preliminary analysis of Niu et al. (2021) and the very recent observational result (Anna-Thomas et al. 2022). On the other hand, under the assumption that the plasma screen's magnetic energy originates from the activities in the magnetosphere of a neutron star, the brightness of the PRS will fade with time as the nebula expands. Thus, FRB sources with compact PRSs might be very young, as proposed in some previous works (e.g., Margalit & Metzger 2018; Zhao & Wang 2021).

We thank the anonymous referee for helpful comments and suggestions. We also thank Siyao Xu for the constructive discussion about the MHD turbulence and Jonathan Katz, Kohta Murase, Yuan-Hong Qu, Fa-Yin Wang, and Zhao-Yang Xia for helpful discussions. This work has been supported by National Natural Science Foundation of China grant Nos. 12003028 and 11988101 and the China Manned Space Project (CMS-CSST-2021-B11). W.L. is supported by a Lyman Spitzer, Jr., Fellowship at Princeton University. Y.F. is supported by Key Research Project of Zhejiang Lab No. 2021PE0AC03.

### ORCID iDs

Yuan-Pei Yang  <https://orcid.org/0000-0001-6374-8313>  
 Wenbin Lu  <https://orcid.org/0000-0002-1568-7461>  
 Yi Feng  <https://orcid.org/0000-0002-0475-7479>  
 Bing Zhang  <https://orcid.org/0000-0002-9725-2524>  
 Di Li  <https://orcid.org/0000-0003-3010-7661>

### References

- Anna-Thomas, R., Connor, L., Burke-Spolaor, S., et al. 2022, arXiv:2202.11112
- Beloborodov, A. M. 2017, *ApJL*, 843, L26
- Beniamini, P., & Kumar, P. 2020, *MNRAS*, 498, 651
- Beniamini, P., Kumar, P., & Narayan, R. 2021, *MNRAS*, 510, 4654
- Bhardwaj, M., Gaensler, B. M., Kaspi, V. M., et al. 2021, *ApJL*, 910, L18
- Bochenek, C. D., Ravi, V., Belov, K. V., et al. 2020, *Natur*, 587, 59
- Chatterjee, S., Law, C. J., Wharton, R. S., et al. 2017, *Natur*, 541, 58
- Chen, G., Ravi, V., & Hallinan, G. W. 2022, arXiv:2201.00999
- CHIME/FRB Collaboration, Andersen, B. C., Bandura, K. M., et al. 2020, *Natur*, 587, 54
- Coles, W. A., Fehlich, R. G., Rickett, B. J., & Codona, J. L. 1987, *ApJ*, 315, 666
- Cordes, J. M., & Chatterjee, S. 2019, *ARA&A*, 57, 417
- Cordes, J. M., Wharton, R. S., Spitler, L. G., Chatterjee, S., & Wasserman, I. 2016, arXiv:1605.05890
- Dai, Z. G., Wang, J. S., & Yu, Y. W. 2017, *ApJL*, 838, L7
- Feng, Y., Li, D., Yang, Y.-P., et al. 2022, *Sci*, 375, 1266
- Fong, W.-F., Dong, Y., Leja, J., et al. 2021, *ApJL*, 919, L23
- Gruzinov, A., & Levin, Y. 2019, *ApJ*, 876, 74
- Hessels, J. W. T., Spitler, L. G., Seymour, A. D., et al. 2019, *ApJL*, 876, L23
- Hilmarsson, G. H., Michilli, D., Spitler, L. G., et al. 2021a, *ApJL*, 908, L10
- Hilmarsson, G. H., Spitler, L. G., Main, R. A., et al. 2021b, *MNRAS*, 508, 5354
- Kashiyama, K., & Murase, K. 2017, *ApJL*, 839, L3
- Kato, T. N. 2007, *ApJ*, 668, 974
- Katz, J. I. 2016, *ApJ*, 826, 226
- Katz, J. I. 2018, *PrPNP*, 103, 1
- Katz, J. I. 2021, *MNRAS*, 501, L76
- Katz, J. I. 2022, *MNRAS*, 510, L42
- Kirsten, F., Marcote, B., Nimmo, K., et al. 2022, *Natur*, 602, 585
- Kremer, K., Piro, A. L., & Li, D. 2021, *ApJL*, 917, L11
- Kumar, P., Lu, W., & Bhattacharya, M. 2017, *MNRAS*, 468, 2726
- Kumar, P., Shannon, R. M., Lower, M. E., et al. 2022, *MNRAS*, Advance Access
- Lanman, A. E., Andersen, B. C., Chawla, P., et al. 2022, *ApJ*, 927, 59
- Li, C. K., Lin, L., Xiong, S. L., et al. 2021a, *NatAs*, 5, 378
- Li, D., Dickey, J. M., & Liu, S. 2019, *RAA*, 19, 016
- Li, D., Wang, P., Qian, L., et al. 2018, *IMMag*, 19, 112
- Li, D., Wang, P., Zhu, W. W., et al. 2021b, *Natur*, 598, 267
- Li, Q.-C., Yang, Y.-P., & Dai, Z.-G. 2020, *ApJ*, 896, 71
- Li, X. J., Dong, X. F., Zhang, Z. B., & Li, D. 2021c, *ApJ*, 923, 230
- Lorimer, D. R., Bailes, M., McLaughlin, M. A., Narkevic, D. J., & Crawford, F. 2007, *Sci*, 318, 777
- Lu, W., Beniamini, P., & Kumar, P. 2022, *MNRAS*, 510, 1867
- Lu, W., Kumar, P., & Zhang, B. 2020, *MNRAS*, 498, 1397
- Luo, R., Wang, B. J., Men, Y. P., et al. 2020, *Natur*, 586, 693
- Margalit, B., Beniamini, P., Sridhar, N., & Metzger, B. D. 2020, *ApJL*, 899, L27
- Margalit, B., Berger, E., & Metzger, B. D. 2019, *ApJ*, 886, 110
- Margalit, B., & Metzger, B. D. 2018, *ApJL*, 868, L4
- Melrose, D. B., & Luo, Q. 2004, *MNRAS*, 352, 915
- Mereghetti, S., Savchenko, V., Ferrigno, C., et al. 2020, *ApJL*, 898, L29
- Metzger, B. D., Berger, E., & Margalit, B. 2017, *ApJ*, 841, 14
- Metzger, B. D., Margalit, B., & Sironi, L. 2019, *MNRAS*, 485, 4091
- Michilli, D., Seymour, A., Hessels, J. W. T., et al. 2018, *Natur*, 553, 182
- Murase, K., Kashiyama, K., & Mészáros, P. 2016, *MNRAS*, 461, 1498
- Nimmo, K., Hewitt, D. M., Hessels, J. W. T., et al. 2021, arXiv:2111.01600
- Niu, C. H., Aggarwal, K., Li, D., et al. 2021, arXiv:2110.07418
- Petroff, E., Hessels, J. W. T., & Lorimer, D. R. 2019, *A&ARv*, 27, 4
- Piro, A. L., & Gaensler, B. M. 2018, *ApJ*, 861, 150
- Piro, L., Bruni, G., Troja, E., et al. 2021, *A&A*, 656, L15
- Pleunis, Z., Good, D. C., Kaspi, V. M., et al. 2021, *ApJ*, 923, 1
- Popov, S. B., & Postnov, K. A. 2013, arXiv:1307.4924
- Qiu, H., Shannon, R. M., Farah, W., et al. 2020, *MNRAS*, 497, 1382
- Quataert, E., & Gruzinov, A. 2000, *ApJ*, 545, 842
- Ravi, V., Law, C. J., Li, D., et al. 2021, arXiv:2106.09710
- Reynolds, S. P., Gaensler, B. M., & Bocchino, F. 2012, *SSRv*, 166, 231
- Rickett, B. J. 1990, *ARA&A*, 28, 561
- Ridnaia, A., Svinin, D., Frederiks, D., et al. 2021, *NatAs*, 5, 372
- Rybicki, G. B., & Lightman, A. P. 1979, *Radiative Processes in Astrophysics* (New York: Wiley)
- Simard, D., & Ravi, V. 2021, arXiv:2107.11334
- Spitkovsky, A. 2008, *ApJL*, 682, L5
- Tavani, M., Casentini, C., Ursi, A., et al. 2021, *NatAs*, 5, 401
- Tendulkar, S. P., Bassa, C. G., Cordes, J. M., et al. 2017, *ApJL*, 834, L7
- The CHIME/FRB Collaboration, Amiri, M., et al. 2021, arXiv:2106.04352
- Vedantham, H. K., & Ravi, V. 2019, *MNRAS*, 485, L78
- Wadiasingh, Z., Beniamini, P., Timokhin, A., et al. 2020, *ApJ*, 891, 82
- Wang, F. Y., Wang, Y. Y., Yang, Y.-P., et al. 2020, *ApJ*, 891, 72
- Wang, W.-Y., Yang, Y.-P., Niu, C.-H., Xu, R., & Zhang, B. 2022, *ApJ*, 927, 105
- Xiao, D., Wang, F., & Dai, Z. 2021, *SCPMA*, 64, 249501
- Xu, H., Niu, J. R., Chen, P., et al. 2021, arXiv:2111.11764
- Xu, S., & Zhang, B. 2016, *ApJ*, 832, 199
- Xu, S., & Zhang, B. 2017, *ApJ*, 835, 2



- Yang, Y.-P., Li, Q.-C., & Zhang, B. 2020, [ApJ](#), 895, 7
- Yang, Y.-P., & Zhang, B. 2017, [ApJ](#), 847, 22
- Yang, Y.-P., & Zhang, B. 2018, [ApJ](#), 868, 31
- Yang, Y.-P., & Zhang, B. 2021, [ApJ](#), 919, 89
- Yang, Y.-P., Zhang, B., & Dai, Z.-G. 2016, [ApJL](#), 819, L12
- Zhang, B. 2020, [Natur](#), 587, 45
- Zhang, B. 2022, [ApJ](#), 925, 53
- Zhao, Z. Y., & Wang, F. Y. 2021, [ApJL](#), 923, L17
- Zhao, Z. Y., Zhang, G. Q., Wang, Y. Y., Tu, Z.-L., & Wang, F. Y. 2021, [ApJ](#), 907, 111
- Zhong, S.-Q., Dai, Z.-G., Zhang, H.-M., & Deng, C.-M. 2020, [ApJL](#), 898, L5